Unveiling the Growth of Polyamide Nanofilm at Water/Organic Free Interface: Towards Enhanced Water/Salt Selectivity

Shenghua Zhou,[†] Li Long,[†] Zhe Yang,[†] Sik Lui So,[†] Bowen Gan,[†] Hao Guo,[*,†] Shien-Ping Feng,[‡] and Chuyang Y. Tang[*,†]

† Department of Civil Engineering, The University of Hong Kong, Pokfulam, Hong Kong SAR 999077, China.

‡ Department of Mechanical Engineering, The University of Hong Kong, Pokfulam, Hong Kong SAR 999077, China.

Corresponding authors:

Dr. Hao Guo, (Email address: guohao7@hku.hk)

Prof. Chuyang Y. Tang, (Email address: tangc@hku.hk)

ABSTRACT

The permeance and selectivity of a reverse osmosis (RO) membrane are governed by its ultrathin polyamide film, yet the growth of this critical film during interfacial polymerization (IP) has not been fully understood. This study investigates the evolution of a polyamide nanofilm at the aqueous/organic interface over time. Despite that its thickness remained largely constant (~15 nm) for IP reaction time ranging from 0.5 to 60 min, the density of polyamide nanofilm increased from 1.25 to 1.36 g cm^{-3} due to the continued reaction between diffused *m*-phenylenediamine (MPD) and dangling acyl chloride groups within the formed polyamide film. This continued growth of the polyamide nanofilm led to a simultaneous increase in its crosslinking degree (from 50.1% to 94.3%) and the healing of nanosized defects, resulting in a greatly enhanced rejection of 99.2 % for NaCl without sacrificing water permeance. Using humic acid as a molecular probe for sealing membrane defects, the relative contributions of the increased crosslinking and reduced defects toward better membrane selectivity were resolved, which supports our conceptual model involving both enhanced size exclusion and healed defects. The fundamental insights on the growth mechanisms and structure-property relationship of the polyamide nanofilm provide crucial guidance for the further development and optimization of high-performance RO membranes.

KEYWORDS: Reverse osmosis, growth of polyamide nanofilm, crosslinking, defects, selectivity.

SYNOPSIS: This study unravels the evolution of the physiochemical properties of a polyamide nanofilm during interfacial polymerization, revealing the fundamental mechanisms governing the structure and separation performance of this critical barrier.

TABLE OF CONTENT

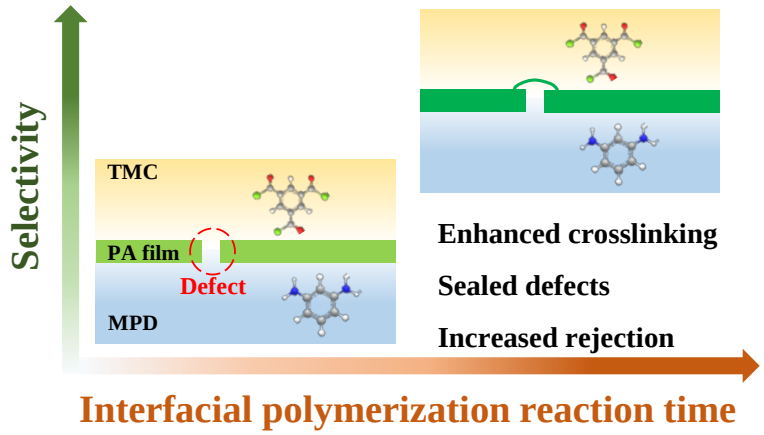

INTRODUCTION

Increasing demand for clean water necessitates technology development to produce fresh water from non-conventional sources, e.g., through desalination and water reuse.[1-4] These applications typically employ thin film composite (TFC) reverse osmosis (RO) membranes, composed of a polyamide active layer, a porous substrate, and a non-woven fabric support.[5-7] Among the different layers, the dense polyamide nanofilm plays the most critical role in the membrane separation performance.[8-10] Numerous studies have focused on enhancing membrane permeance by fabricating thinner polyamide nanofilms,[11-14] tuning their surface morphology,[15-17] and incorporating additional nanochannels.[18-20] Unfortunately, enhancement in permeance is often accompanied with sacrificed selectivity, a phenomenon commonly known as the permeance-selectivity tradeoff or the "upper bound".[8, 9, 21, 22]

Compared to water permeance, many recent studies have reported the greater importance of selectivity on the overall performance of RO plants.[23] Membranes with high selectivity not only improves product water quality but also eliminates the need for additional treatment steps (such as a second-pass RO for seawater desalination).[24] It has been well documented that the selectivity of an RO membrane is strongly influenced by the crosslinking degree[25, 26] (and thus the effective pore size[27, 28]) of its polyamide nanofilm. Nevertheless, the evolution of crosslinking degree during the growth of this nanofilm is still poorly understood. In addition, membrane selectivity could be adversely affected by nanosized defects.[29] Despite the sub-nanometer pore size of typical polyamide films (2.1-4.5 Å in radii based on free volume characterization[28, 30]), RO membranes generally show incomplete rejection of viruses, giant molecules and bacteria (e.g., 3.4 to 7 log removal for MS2 phage of ~25 nm,[31] 3 to ≥ 4 log removal for supercoiled plasmid DNA of ~70 nm,[32] and 4.5 to > 5.7 log removal for *C. parvum* of ~5 μm[33]). Song et al. attributed this non-ideal rejection behavior to the inherent tendency to

form nanosized defects during the interfacial polymerization (IP) of polyamide films.[34] Despite the critical role of nanosized defects in separation performance of polyamide membranes, the formation and evolution of these defects during IP have not been systematically investigated, which prompts us to explore the fundamental mechanisms as well as the inherent relationship between membrane integrity and selectivity.

The difficulty to resolve the growth mechanism and defect formation in conventional IP is at least partially caused by the ridge-and-valley surface roughness features of typical polyamide RO membranes.[35, 36] To avoid such interferences, we adopt a novel free interface fabrication strategy to form smooth polyamide nanofilms by suppressing the nanofoaming-induced surface roughness.[11, 13, 14, 37-40] The series of smooth polyamide films formed over predetermined time steps enable us to unravel the evolution of their physiochemical properties (e.g., thickness, density, crosslinking degree, and defects) as well as correlate these properties to membrane separation performance. These fundamental insights into the growth dynamics of polyamide rejection films and their structure-performance correlation provide important guidance to the future development of high-performance RO membranes.

EXPERIMENTAL SECTION

Chemicals.

M-phenylenediamine (MPD, 99%), trimesoyl chloride (TMC, 98%), and *n*-hexane (95%) from Sigma-Aldrich were used for the fabrication of polyamide nanofilms. Sodium chloride (NaCl, Dieckmann), sodium hydroxide (NaOH, Dieckmann), and hydrochloric acid (HCl, 37%, VWR) were used to adjust solution chemistry. Silver nitrate ($AgNO_3$, Sigma-Aldrich) and nitric acid (HNO_3, 69%, VWR) were used to determine the content of carboxylic groups in polyamide layer. Humic acid (HA, Sigma-Aldrich) was used for membrane defect healing. Boron (in the form of boric acid ($B(OH)_3$)) and xylitol were used to test film rejection of neutral molecules. Unless specified otherwise, all the aqueous solutions were prepared using Milli-Q water.

Polyamide nanofilm fabrication.

A free interface fabrication strategy was adopted to prepare the polyamide nanofilms using a custom-designed interfacial polymerization cell (Figure S1, Supporting Information S1). Briefly, a 30 mL aqueous solution with 2.0 wt. % MPD was introduced into the cell first. Subsequently, a 10 mL hexane solution containing 0.1 wt. % TMC was gently added on the surface of aqueous solution to allow the IP reaction occurred at the aqueous/organic interface for a duration of 0.5-60 min. The fabricated polyamide nanofilm was deposited onto a preloaded polysulfone substrate by the vacuum-assisted drainage of MPD solution (Figure S2).[38, 41] This substrate (molecular weight cut-off of 67 kDa, Vontron Membrane Technology) comprises a porous polysulfone layer of ~40-45 μm in thickness, which is further supported by a non-woven fabric to provide enhanced mechanical strength. Additional information of the substrate, such as its appearance and surface wettability, can be found in Supporting Information S2. Residual TMC/hexane solution on the membrane surface was then removed

by a thorough rinsing using hexane. The resultant membrane was denoted as RO-*n*, where *n* represents the duration of IP reaction.

Traditional TFC membrane fabrication.

For comparison purpose, we also fabricated a TFC polyamide film by performing the traditional IP reaction directly on a polysulfone substrate. Other fabrication conditions were identical to those used for RO-1, i.e., a 2.0 wt. % MPD solution and a 0.1 wt. % TMC solution for the IP reaction with 1 min.

Nanofilm characterization.

The surface morphology of polyamide nanofilm was characterized by a field-emission scanning electron microscope (FE-SEM, S-4800, Hitachi). All the samples were dried and sputter coated with a thin gold layer before SEM characterization. A transmission electron microscope (TEM, G2, FEI Tecnai) was used to resolve their cross-sectional structure. Nanofilm thickness was determined by an atomic force microscope (AFM, Dimension 3100, Vecco) with a scan rate of 6 Hz. The density of polyamide nanofilm was calculated by its thickness and determined mass using a quartz crystal microbalance (QCM, Q-Sense E4, Biolin Scientific, Supporting Information S3).[13, 42, 43] The crosslinking degree of nanofilm was calculated by the determined O/N ratio using an X-ray photoelectron spectroscopy (XPS, Axis Ultra Dld, Supporting Information S4).[19, 44, 45] The water contact angle was evaluated using a contact angle analyzer (Attention Theta, Biolin Scientific). The charged carboxyl group content within the polyamide nanofilm was determined at pH 10.5 using an $AgNO_3$-based titration method (Supporting Information S5). Silver ions could preferentially bind to charged

(deprotonated) carboxyl groups.[46, 47] Subsequently, nitric acid was used to elute the bound silver ions. Finally, inductively coupled plasma spectrometry (ICP-MS, Agilent 7900) was utilized to detect the concentration of silver ions for the calculation of the charged carboxyl group density. It should be noted that the number of charged carboxylate groups is affected by the pH of the $AgNO_3$ solution. According to the literature,[46, 47] carboxyl groups are expected to be fully deprotonated at pH 10.5, so the charged carboxyl group content within the polyamide nanofilm was determined at pH 10.5 in the current study. Doppler broadening energy spectroscopy (DBES, Institute of High Energy Physics, Chinese Academy of Sciences) was used to characterize the *S* parameter of RO-1 and RO-60 films. DBES can reflect the information of free-volume of the polyamide nanofilm at an atomic scale (e.g., 0.2-2 nm) through positron annihilation.[28, 48] The *S* parameter represents the ratio of the counts in the energy range of 510.2-511.8 keV to the total counts (within 499.5-522.5 keV),[49] and its value is sensitive to the change of the positron states caused by nano-structural changes. When the positron is localized in a free volume with a finite size, the observed *S* parameter is a measure of the momentum broadening according to the uncertainty principle: a larger free volume could result in a larger *S* parameter value.[48-50] The DBES characterization was operated using a positron source of ^{22}Na with the positron energy range of 0-5 keV.

Separation performance.

The separation performance of polyamide nanofilms was tested on a laboratory scale crossflow filtration setup.[11] A testing coupon consisting of a polyamide nanofilm and a polysulfone support was installed into the crossflow filtration cell with an effective filtration area of 12 cm^2. The coupon was then pre-compacted with a 5 L feed solution containing DI water, 2000 ppm

NaCl, 5 ppm boron (in the form of boric acid ($B(OH)_3$)), 200 ppm xylitol, 2000 ppm MPD, or 100 ppm HA at 17.5 bar under 25 °C for 1 h. Samples were then collected to determine the water flux and solute rejections of polyamide nanofilms. Water flux (J_w) and water permeance (A) were calculated by:

$$J_w = \frac{\Delta m}{\Delta t \times a \times \rho} \quad (1)$$

$$A = \frac{J_W}{\Delta P - \Delta \pi} \quad (2)$$

where Δm is the mass of permeate water over the sample collection duration of Δt, a is the effective filtration area (i.e., 12 cm^2), ρ is the density of water (i.e., 1 g cm^{-3}), ΔP is the applied hydraulic pressure, and $\Delta \pi$ is the osmotic pressure between feed solution and permeate solution. Solute rejection (R) and solute permeability (B) were determined by:

$$R = \frac{C_f - C_p}{C_f} \quad (3)$$

$$B = \frac{1-R}{R} J_W \quad (4)$$

where C_f and C_p are the solute concentrations in feed and permeate solution, respectively. NaCl concentration was measured by a portable conductivity meter (Myron II). The concentration of MPD was determined using an ultraviolet-visible spectrophotometer (UV, UH-5300, Hitachi). HA and xylitol concentrations were tested by a total organic carbon (TOC) analyzer (TOC-L CPH, SHIMADZU). The concentration of boron was detected by an ICP-MS (Agilent 7900).

Defect healing.

A vacuum-assisted deposition of HA was developed to partially heal the intrinsic defects within the polyamide nanofilms. Briefly, a polyamide nanofilm was preloaded on a polysulfone substrate following by the addition of 50 mL 1 ppm HA solution. The healing process was performed by vacuum filtration of the HA solution at a vacuum pressure of ~ 1 bar for 1 min. The healed nanofilms were thoroughly rinsed by Milli-Q water to remove residual HA. Their

separation performance was then systematically evaluated following the same protocol in the previous section.

RESULTS AND DISCUSSION

Microscopic morphology.

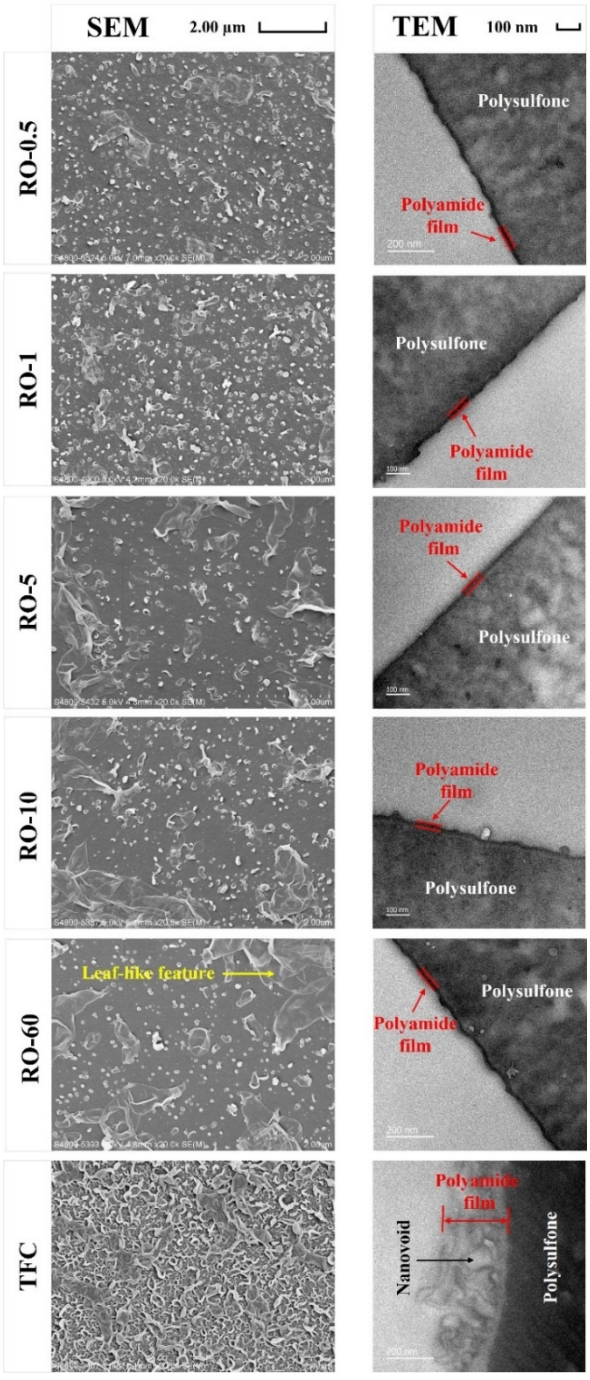

Figure 1. The surface SEM micrographs and cross-sectional TEM micrographs of polyamide films with different IP times (0.5 min, 1 min, 5 min, 10 min and 60 min). The micrographs of a TFC

polyamide film fabricated by performing traditional IP process (1 min reaction time) on a polysulfone substrate with otherwise identical conditions (2.0 wt. % MPD and 0.1 wt. % TMC) were also included for comparison purpose. The relative darkness in TEM micrographs is related to the relative mass density, with higher mass density showing darker color. For the membranes formed at free interface (RO-0.5, RO-1, RO-5, RO-10, and RO-60), their polyamide layers are darker than their polysulfone substrates due to the crosslinked nature of the polyamide layers. For the traditional TFC membrane, the polyamide layer had a lighter color as a result of extensive presence of nanovoids inside its polyamide layer,[36] which reduces the effective mass density.

Figure 1 shows the surface (SEM) and cross-sectional (TEM) morphology of the polyamide films prepared with different IP times. As expected, the adoption of the free-interface strategy (RO-0.5, RO-1, RO-5, RO-10, and RO-60) successfully suppressed the formation of "ridge-and-valley" appearance that is typical for traditional IP (TFC), resulting in relatively smooth surfaces of the polyamide films. Similar low-roughness films have also been reported in the literatures,[13, 14, 38] which has been attributed to the weakened local heating[14, 51] and reduced confinement effect[37, 38] during IP reaction in the absence of substrate. This relatively smooth surface morphology enables us to evaluate the evolution of the film thickness over time (Figure 2 AFM).

AFM measurements show that the film thickness was typically in the range of 14.5-15.6 nm over time (Figure 2). To verify the statistical significance of the difference in thickness for RO-60 and RO-0.5, we conducted a Student's t-test for the data. The results show a p value of < 0.02 for RO-60 vs. RO-0.5, suggesting that the difference in thickness for the two polyamide films is statistically significant. Nevertheless, the growth in film thickness over time was very slow after $t = 0.5$ min. Our experimental observations appear to be in line with Freger's and Dickson et al.'s simulation studies[52, 53] that the formation of a nascent polyamide film would dramatically slow down the diffusion of MPD monomers from the aqueous phase to the organic phase, thereby retarding the subsequent growth of the polyamide film. Nevertheless, a few studies reported substantial growth of polyamide layer over time,[54, 55] e.g., from ~40 to 110 nm when the IP reaction time was increased from 10 sec to 600 sec.[55] This contradiction could be

potentially reconciled by the difference in the definition of intrinsic vs. apparent film thickness.[34] Conventional polyamide films formed by traditional IP generally show a ridge-and-valley roughness structure containing numerous nanovoids[11, 56] (around 30% by volume fraction obtained from TEM images[57]). Song et al.[34] studied the polyamide morphology of four commercial RO membranes and found that despite the major difference in the apparent thicknesses of their rejection layers, their intrinsic thicknesses were all in the range of 10-20 nm, which is in line with the film thickness (~15 nm in Figure 2) observed in the current study.[58-61]

The SEM micrographs in Figure 1 show the emergence and growth of some leaf-like features on the surface of polyamide nanofilms at longer IP reaction times. This morphological change is probably caused by the leakage of amine monomers through nanosized defects of the polyamide films: the convection of the MPD solution through a defect and its reaction with TMC in the organic phase forms a “leaf”. In a previous study, Song et al.[38] observed nanosized pinholes at the bottom surface of a polyamide film formed at a free interface, and these pinholes seem to be co-located with leaf-like features. This explanation is also consistent with Grzebyk et al.’s observation on the growth of additional roughness features over an existing polyamide film (e.g., a commercial RO membrane): the formation of additional leaf-like roughness feature is well correlated to the transport of MPD across the existing layer.[62] Presumably, the presence of defects would allow a faster localized MPD supply, which would promote the further growth of polyamide near the defective regions.

To verify the existence of defects, we performed filtration tests using Aldrich HA. According to Song et al.,[34] the macromolecular size of HA (approximately 1.1-5.4 nm[63]) together with its soft property could allow it to penetrate through the defects but not through an intact polyamide

film. These features could enable HA to be used to verify nanosized defects. It is worthwhile to note that HA and other macromolecules have also been commonly used to partially seal membrane defects.[64-66] Figure S7 shows HA rejection of below 97%, which confirms the presence of defects in the polyamide nanofilms. Song et al.[34] also shows the presence of defects in commercial RO membranes based on HA tracer tests: their TEM characterization confirms that the colloidal HA molecules were able to penetrate through a polyamide layer into the polysulfone substrate. The existence of nanosized defects would allow the convection of amine monomers through the polyamide nanofilms, whose reaction with TMC monomers forms leaf-like features. Such secondary growth of leaf-like features over the defective regions tends to partially heal the defects, as reflected by the reduced passage of HA at longer IP rection time (Figure S7). The implications of the formation and evolution of defects on membrane rejection will be further discussed in the section "Membrane separation performance".

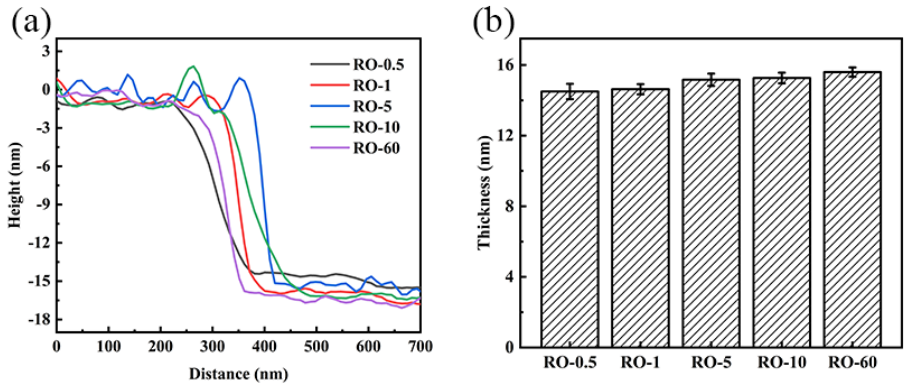

Figure 2. AFM characterization of polyamide films with different IP times (0.5 min, 1 min, 5 min, 10 min and 60 min). (a) Height profiles of various polyamide nanofilms with different IP reaction times. The height profiles were obtained after polyamide films were transferred into silicon wafers. (b) Thicknesses of polyamide films based on height differences between polyamide films and silicon wafers. The error bars represent the standard deviation based on at least three replicate measurements using different membrane coupons.

Physicochemical properties.

As shown in Figure 3a, increasing IP reaction time led to reduced O/N ratio ($r_{O/N}$), revealing the evolution of polyamide toward greater crosslinking degree (n) over time (e.g., from 50.1% at 0.5 min to 94.3% at 60 min). Extended IP reaction time provides more opportunities for amine monomers to diffuse into/through a polyamide film and to continue reacting with those

unreacted acyl chloride functional groups of the film, which would promote greater crosslinking of polyamide. Consistent to this increase in crosslinking degree over time, the density of charged carboxyl groups (formed by the hydrolysis of unreacted acyl chloride groups after IP reaction) dropped from 22.6 ± 0.8 nm^{-2} for RO-0.5 to 9.2 ± 0.9 nm^{-2} for RO-60 at pH 10.5 (Figure 3b). The reduced number of charged carboxyl groups also led to an increase in water contact angle, noting that the charged carboxyl groups are able to form hydrogen bonds with water molecules and thus can improve film hydrophilicity.[67]

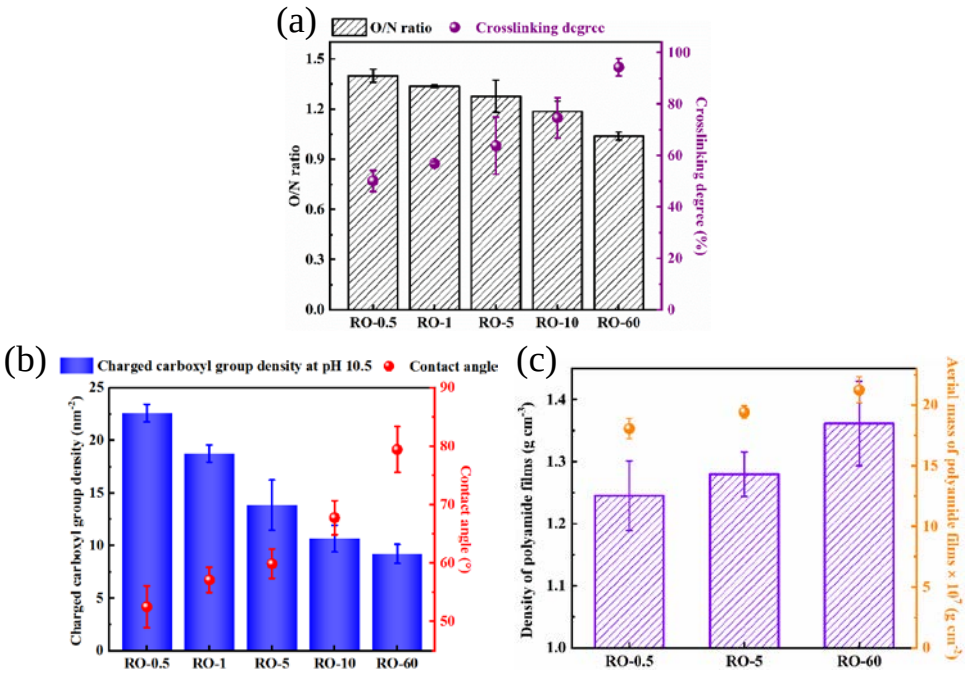

Figure 3. Physicochemical properties of polyamide films. (a) The O/N ratio ($r_{O/N}$) and crosslinking degree (n) of polyamide films. The O/N ratio was used to calculate crosslinking degree of a polyamide film based on the equation: $n = (4 - 2r_{O/N})/(1 + r_{O/N})$.[13] (b) Charged carboxyl group density and water contact angles of various polyamide films. Charged carboxyl group density of polyamide was quantified by a silver binding method in accordance with Ref. 46, 47 at pH 10.5. (c) Density and aerial mass of different polyamide films (RO-0.5, RO-5 and RO-60). The density of polyamide film was determined based on the thickness measured by AFM and the film mass measured by a quartz crystal microbalance. The error bars represent the standard deviation based on at least three replicate measurements using different membrane coupons.

Figure 3c shows significantly increased polyamide film density over longer IP reaction time (1.25 ± 0.06 g cm^{-3} at 0.5 min vs. 1.36 ± 0.07 g cm^{-3} at 60 min, $p < 0.04$). Despite that the film thickness was only marginally increased (Figure 2), QCM results show increased aerial mass from 1.81 × 10^{-6} g cm^{-2} at 0.5 min to 2.12 × 10^{-6} g cm^{-2} at 60 min (Figure 3c), which confirms the continued IP reaction over time. Consistent with the increased crosslinking degree, MPD

molecules diffused into a polyamide film can react with dangling acyl chloride groups within the film to result in higher film density. This growth of a denser film is in addition to (1) the diffusion of MPD through the film whose reaction with TMC in the organic phase would increase the film thickness (Figure 2) and (2) the convection of MPD through the defects of the film whose reaction forms leaf-like features to heal defects (SEM, Figure 1). The evolution of the polyamide nanostructure over time has major implications on its separation properties, which is further discussed in the section "Membrane separation performance".

Membrane separation performance.

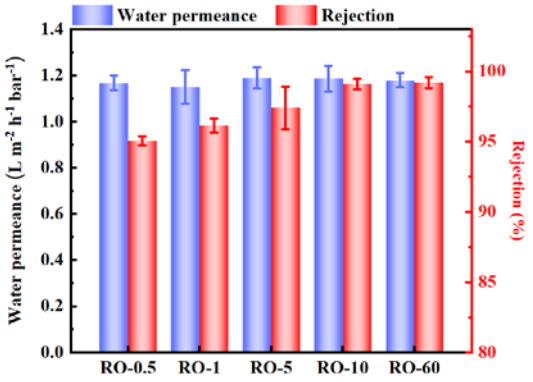

Figure 4. Water permeance and NaCl rejection of polyamide films with different IP times (0.5 min, 1 min, 5 min, 10 min and 60 min). Testing conditions: DI water (for pure water permeance measurements) or 2000 ppm NaCl (for salt rejection measurements) at 17.5 bar with the crossflow velocity of 22.4 cm/s under room temperature (25 °C). The effective filtration area of the crossflow filtration cell is 12 cm^2. The coupon was pre-compacted with feed solution (5 L) to achieve stable separation performance. The error bars represent the standard deviation based on at least three replicate measurements using different membrane coupons.

Extending IP reaction time had little effect on water permeance (Figure 4). In contrast, the NaCl rejection increased from 95.0% to 99.2% when the IP reaction time was extended from 0.5 min to 60 min. The enhanced salt rejection can be at least partially attributed to the improved film crosslinking (Figure 3a).[25] In the current study, we show that this improvement in crosslinking of a polyamide film corresponds to an increased density of the film (Figure 3c), which could enhance the size exclusion effect[27, 28] and result in a more selective polyamide rejection layer. In addition, healing of nanosized defects at longer IP time (Figure 5) is also

expected to improve NaCl rejection. To further confirm the role of defects on membrane rejection, we performed additional salt rejection tests for films treated with mild HA fouling (Figure 5a). According to prior studies,[64] HA macromolecules could partially plug nanosized defects of polyamide films, thereby improving film rejection. Figure 5 shows obviously improved NaCl rejection and water-NaCl selectivity after HA treatment, confirming impaired rejection and selectivity due to defects in films with short IP times (e.g., 0.5 and 1 min). At extended IP time of 10 and 60 mins, little difference in NaCl rejection could be observed before and after HA treatment, which is consistent with less defects in these films at longer IP reaction time. Figure 5 further allows us to resolve the role of size exclusion effect from that of defects: longer IP time resulted in better rejection and selectivity even for the HA-treated films (e.g., higher NaCl rejection (99.4%) by HA-treated RO-60 than those of HA-treated RO-0.5 (96.8%) and RO-1 (97.9%)), once again confirming the critical role of size exclusion for more crosslinked polyamide films.

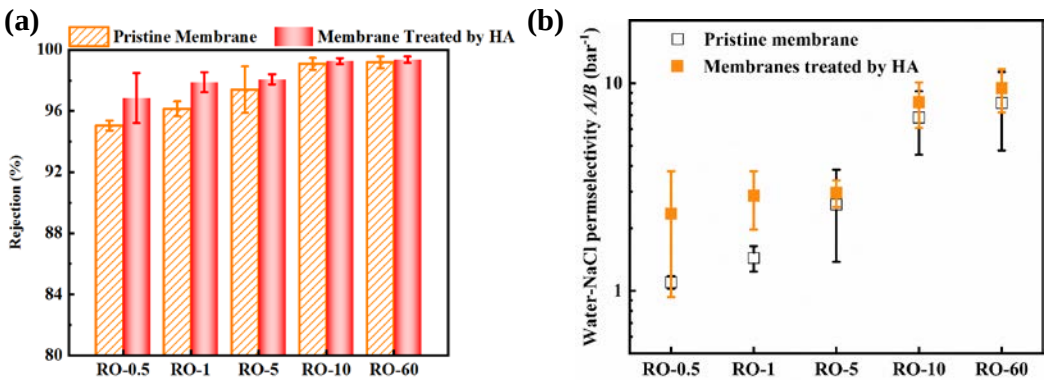

Figure 5. Separation performance comparison of polyamide films with different IP times (0.5 min, 1 min, 5 min, 10 min and 60 min) before/after HA treatment. (a) NaCl rejection (2000 ppm) comparison of polyamide films before/after HA treatment. (b) Water-NaCl permselectivity of polyamide films before/after HA treatment. HA treatment was performed by depositing HA onto polyamide films by using vacuum filtration. The volume of HA solution was 50 mL. The concentration of HA solution was 1 ppm, and the filtration time was 1 min. The error bars represent the standard deviation based on at least three replicate measurements using different membrane coupons.

Conceptual model.

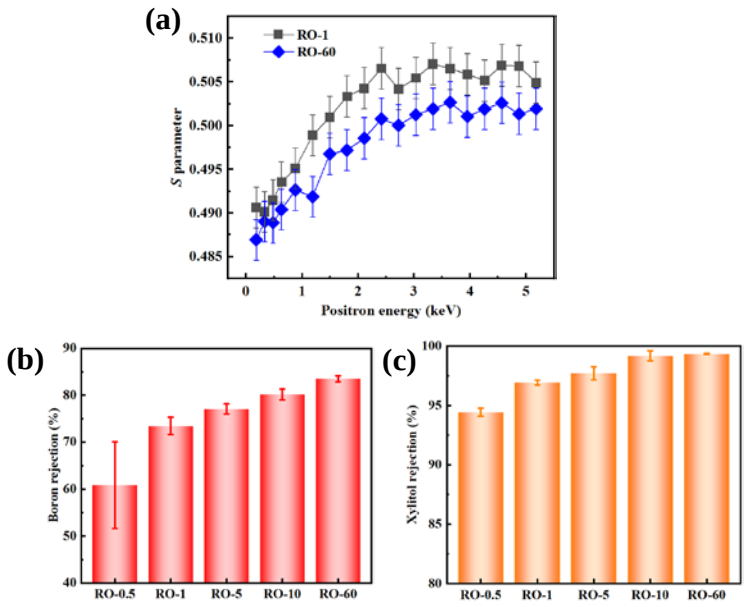

Figure 6. (a) *S* parameter of RO-1 and RO-60 nanofilms tested by DBES, and rejection of (b) boron and (c) xylitol by polyamide films with different IP times (0.5 min, 1 min, 5 min, 10 min and 60 min). The effective filtration area of the crossflow filtration cell is 12 cm^2. The coupon was pre-compacted with feed solution (5 L) to achieve stable separation performance. The error bars represent the standard deviation based on at least three replicate measurements using different membrane coupons.

To further understand the evolution of effective pore size and free volume of the nanofilms over time, we performed DBES characterization for RO-1 and RO-60. Our DBES results (Figure 6a) are in line with the reported range of *S* parameters (0.48-0.53) in the literature.[27, 51] Since a larger *S* value indicates a greater free volume in the polyamide film,[50, 51] the lower *S* parameter of RO-60 confirmed the reduced free volume inside the polyamide layer over longer IP reaction time, which is consistent with the film crosslinking and density measurements (Figure 3). Additional rejection tests were also performed for neutral molecules boron (in the form of boric acid) and xylitol. Since the rejection of these molecules is not affected by electrostatic interactions, their rejection behaviors allow a better understanding of the size exclusion effect. Figure 6b,c shows improved rejection of both molecules over longer IP reaction time, which confirms the reduced effective pore size over time. The extended IP reaction time would provide more opportunities for amine groups to react with acyl chloride groups within the polyamide nanofilm, which increases the crosslinking degree and the film

density as well as decreases the free volume and effective pore size. In addition to the enhanced size exclusion effect, healing of defects in polyamide over longer reaction time may have also contributed to the improved rejection of the neutral molecules. It has been reported that IP reactions can potentially lead to the formation of nanosized defects.[34, 68] Presumably, the presence of defects would allow a faster localized transport of amine monomers, whose subsequent reaction with TMC in the organic phase tends to partially heal the defects. We further evaluated the rejection of MPD by the different polyamide films. The transport of MPD across the polyamide films could provide additional information to better understand the evolution of polyamide films over time. As shown in Figure 7, the polyamide films formed at longer IP reaction time achieved less passage for MPD monomers. Since the growth in the film thickness is dependent on the supply of MDP monomers,[54, 62, 69] the reduced transport rate of MPD at longer IP reaction time explains the limited growth of film thickness over time. This "self-limit" nature of film growth is critical for the formation of ultrathin polyamide films, commonly in the range of 10-20 nm as reported in the literatures[58-61] for RO membranes. Furthermore, the reduced MPD passage is consistent with our conceptual model involving increased crosslinking and improved defect healing over longer reaction time. On the other hand, our experimental results revealed that this evolution in membrane structure did not impair the water permeance (Figure 4), making it a potentially attractive strategy for the synthesis of high-performance RO membranes.

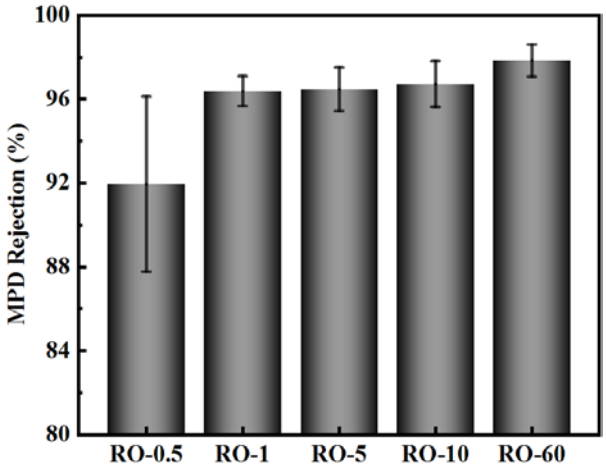

Figure 7. Rejection of MPD by polyamide films with different IP times (0.5 min, 1 min, 5 min, 10 min and 60 min). The effective filtration area of the crossflow filtration cell is 12 cm^2. The coupon was pre-compacted with feed solution (5 L) to achieve stable separation performance. The error bars represent the standard deviation based on at least three replicate measurements using different membrane coupons.

Structure-property correlation.

Table 1. Correlation coefficients of key parameters (IP reaction time, thickness, crosslinking degree, density, water permeance and NaCl rejection) of polyamide films. Due to potential nonlinear reaction kinetics, the correlation was performed on a log-log scale. Microsoft Excel was utilized to analyze the correlation coefficients based on the CORREL function. Correlation on a linear scale is presented in Supporting Information S7 for comparison purpose.

	IP reaction time	Thickness	Crosslinking degree	Density	Water permeance	NaCl rejection
IP reaction time	1	-	-	-	-	-
Thickness	**0.82**	1	-	-	-	-
Crosslinking degree	**0.93**	**0.68**	1	-	-	-
Density	**0.72**	0.41	**0.64**	1	-	-
Water permeance	0.20	-0.02	0.21	0.11	1	-
NaCl rejection	**0.88**	**0.75**	**0.78**	**0.65**	0.08	1

To better understand the structure-property relationship, we performed a correlation analysis among the structural properties and performance parameters for the polyamide films formed at different IP rection time (Table 1). Increasing the reaction time resulted in greater crosslinking degree (correlation coefficient r = 0.93) and film density (r = 0.72), along with a marginal increase in film thickness (r = 0.82). In the current study, the membrane water permeance seems to be poorly correlated to these structural properties. This might be partially explained by the

small differences in the membrane thickness (< 7.1%). Interestingly, enhanced salt rejection could be achieved without sacrificing water permeance (r = 0.08), providing a potential way to overcome the permeance-selectivity trade-off. The NaCl rejection was found to be strongly dependent on the membrane structural parameters (r = 0.75, 0.78, and 0.65 for film thickness, crosslinking degree, and film density, respectively). The strong dependence of NaCl rejection on film thickness is possibly explained by the growth of the secondary leaf-like features at longer IP reaction time, which tends to seal the defects in the polyamide film. At the same time, a denser and more crosslinked rejection layer is favorable to increased NaCl rejection as a result of enhanced size exclusion.

ASSOCIATED CONTENT

Supporting Information

The Supporting Information is available free of charge at https://pubs.acs.org/.

S1. Fabrication of polyimide film by support free interfacial polymerization (IP); S2. The appearance, surface morphology, cross-section, and water contact angle of substrate layer.; S3. Sample preparation for AFM characterization, QCM test, and calculation of film density; S4. Calculation of film crosslinking degree; S5. Calculation of charged carboxyl group content in polyamide nanofilm; S6. Rejection of humic acid (HA) for polyamide films with different IP reaction times; S7. Structure-property correlation.

AUTHOR INFORMATION

Corresponding authors

Hao Guo - Department of Civil Engineering, The University of Hong Kong, Pokfulam, Hong Kong SAR, China; ORCID: 0000-0002-0688-5431; Phone: +852 28578470; Email: guohao7@hku.hk.

Chuyang Y. Tang - Department of Civil Engineering, The University of Hong Kong, Pokfulam, Hong Kong SAR, China; ORCID: 0000-0002-7932-6462; Phone: +852 28591976; Email: tangc@hku.hk.

Authors

Shenghua Zhou - Department of Civil Engineering, The University of Hong Kong, Pokfulam, Hong Kong SAR, China.

Li Long - Department of Civil Engineering, The University of Hong Kong, Pokfulam, Hong Kong SAR, China; ORCID: 0000-0002-7951-3276.

Zhe Yang - Department of Civil Engineering, The University of Hong Kong, Pokfulam, Hong Kong SAR, China; ORCID: 0000-0003-0753-3902.

Sik Lui So - Department of Civil Engineering, The University of Hong Kong, Pokfulam, Hong Kong SAR, China.

Bowen Gan - Department of Civil Engineering, The University of Hong Kong, Pokfulam, Hong Kong SAR, China.

Shien-Ping Feng - Department of Mechanical Engineering, The University of Hong Kong, Hong Kong SAR, China; ORCID: 0000-0002-3941-1363.

Notes

The authors declare no competing financial interest.

ACKNOWLEDGMENTS

This work was fully supported by the Senior Research Fellow Scheme of Research Grants Council (Grant No. SRFS2021-7S04) and Seed Fund for Translational and Applied Research at The University of Hong Kong, China (Grant No. 104006008). We thank Dr. Xiaoxiao Song from Zhejiang University of Technology for his advice on polyamide nanofilm fabrication.

REFERENCES

1. Mekonnen, M. M.; Hoekstra, A. Y., Four billion people facing severe water scarcity. *Sci. Adv.* **2016,** *2*, (2), e1500323.
2. Werber, J. R.; Osuji, C. O.; Elimelech, M., Materials for next-generation desalination and water purification membranes. *Nat. Rev.Mater.* **2016,** *1*, (5), 16018.
3. Elimelech, M.; Phillip, W. A., The future of seawater desalination: energy, technology, and the environment. *Science* **2011,** *333*, (6043), 712-717.
4. Guo, H.; Dai, R.; Xie, M.; Peng, L. E.; Yao, Z.; Yang, Z.; Nghiem, L. D.; Snyder, S. A.; Wang, Z.; Tang, C. Y., Tweak in Puzzle: Tailoring Membrane Chemistry and Structure toward Targeted Removal of Organic Micropollutants for Water Reuse. *Environ. Sci. Technol. Lett.* **2022,** *9*, (4), 247-257.
5. Tang, C. Y.; Yang, Z.; Guo, H.; Wen, J. J.; Nghiem, L. D.; Cornelissen, E., Potable water reuse through advanced membrane technology. *Environ. Sci. Technol.* **2018,** *52*, (18), 10215-10223.
6. Koros, W. J.; Zhang, C., Materials for next-generation molecularly selective synthetic membranes. *Nat. Mater.* **2017,** *16*, (3), 289-297.
7. Liang, C. Z.; Askari, M.; Choong, L. T. S.; Chung, T. S., Ultra-strong polymeric hollow fiber membranes for saline dewatering and desalination. *Nat. Commun.* **2021,** *12*, (1), 2338.
8. Robeson, L. M., Correlation of separation factor versus permeability for polymeric membranes. *J. Membr. Sci.* **1991,** *62*, (2), 165-185.
9. Yang, Z.; Guo, H.; Tang, C. Y., The upper bound of thin-film composite (TFC) polyamide membranes for desalination. *J. Membr. Sci.* **2019,** *590*, 117297.
10. Culp, T. E.; Khara, B.; Brickey, K. P.; Geitner, M.; Zimudzi, T. J.; Wilbur, J. D.; Jons, S. D.; Roy, A.; Paul, M.; Ganapathysubramanian, B.; Zydney, A. L.; Kumar, M.; Gomez, E. D., Nanoscale control of internal inhomogeneity enhances water transport in desalination membranes. *Science* **2021,** *371*, (6524), 72-75.
11. Ma, X. H.; Yao, Z. K.; Yang, Z.; Guo, H.; Xu, Z. L.; Tang, C. Y.; Elimelech, M., Nanofoaming of polyamide desalination membranes to tune permeability and selectivity. *Environ. Sci. Technol. Lett.* **2018,** *5*, (2), 123-130.
12. Chowdhury, M. R.; Steffes, J.; Huey, B. D.; McCutcheon, J. R., 3D printed polyamide membranes for desalination. *Science* **2018,** *361*, (6403), 682-685.
13. Karan, S.; Jiang, Z. W.; Livingston, A. G., Sub-10 nm polyamide nanofilms with ultrafast solvent transport for molecular separation. *Science* **2015,** *348*, (6241), 1347-1351.
14. Jiang, Z.; Karan, S.; Livingston, A. G., Water transport through ultrathin polyamide nanofilms used for reverse osmosis. *Adv. Mater.* **2018,** *30*, (15), e1705973.
15. Tan, Z.; Chen, S. F.; Peng, X. S.; Zhang, L.; Gao, C. J., Polyamide membranes with nanoscale Turing structures for water purification. *Science* **2018,** *360*, (6388), 518-521.
16. Wang, Z.; Wang, Z.; Lin, S.; Jin, H.; Gao, S.; Zhu, Y.; Jin, J., Nanoparticle-templated nanofiltration membranes for ultrahigh performance desalination. *Nat. Commun.* **2018,** *9*, (1), 2004.
17. Yuan, B.; Zhao, S.; Hu, P.; Cui, J.; Niu, Q. J., Asymmetric polyamide nanofilms with highly ordered nanovoids for water purification. *Nat. Commun.* **2020,** *11*, (1), 6102.

18. Di Vincenzo, M.; Tiraferri, A.; Musteata, V. E.; Chisca, S.; Sougrat, R.; Huang, L. B.; Nunes, S. P.; Barboiu, M., Biomimetic artificial water channel membranes for enhanced desalination. *Nat. Nanotechnol.* **2021,** *16*, (2), 190-196.
19. Yang, Z.; Guo, H.; Yao, Z. K.; Mei, Y.; Tang, C. Y., Hydrophilic silver nanoparticles induce selective nanochannels in thin film nanocomposite polyamide membranes. *Environ. Sci. Technol.* **2019,** *53*, (9), 5301-5308.
20. Yin, J.; Yang, Z.; Tang, C. Y.; Deng, B., Probing the contributions of interior and exterior channels of nanofillers toward the enhanced separation performance of a thin-film nanocomposite reverse osmosis membrane. *Environ. Sci. Technol. Lett.* **2020,** *7*, (10), 766-772.
21. Yang, Z.; Long, L.; Wu, C.; Tang, C. Y., High Permeance or High Selectivity? Optimization of System-Scale Nanofiltration Performance Constrained by the Upper Bound. *ACS EST Eng.* **2022,** *2*, (3), 377-390.
22. Ritt, C. L.; Stassin, T.; Davenport, D. M.; DuChanois, R. M.; Nulens, I.; Yang, Z.; Ben-Zvi, A.; Segev-Mark, N.; Elimelech, M.; Tang, C. Y.; Ramon, G. Z.; Vankelecom, I. F. J.; Verbeke, R., The open membrane database: Synthesis–structure–performance relationships of reverse osmosis membranes. *J. Membr. Sci.* **2022,** *641*, 119927.
23. Park, H. B.; Kamcev, J.; Robeson, L. M.; Elimelech, M.; Freeman, B. D., Maximizing the right stuff: The trade-off between membrane permeability and selectivity. *Science* **2017,** *356*, (6343).
24. Werber, J. R.; Deshmukh, A.; Elimelech, M., The critical need for increased selectivity, not increased water Permeability, for desalination membranes. *Environ. Sci. Technol. Lett.* **2016,** *3*, (4), 112-120.
25. Ali, Z.; Al Sunbul, Y.; Pacheco, F.; Ogieglo, W.; Wang, Y.; Genduso, G.; Pinnau, I., Defect-free highly selective polyamide thin-film composite membranes for desalination and boron removal. *J. Membr. Sci.* **2019,** *578*, 85-94.
26. An, X.; Hu, Y.; Wang, N.; Wang, T.; Liu, Z., Breaking the permeability–selectivity trade-off in thin-film composite polyamide membranes with a PEG-b-PSF-b-PEG block copolymer ultrafiltration membrane support through post-annealing treatment. *NPG Asia Mater.* **2019,** *11*, (1), 13.
27. Liang, Y.; Zhu, Y.; Liu, C.; Lee, K. R.; Hung, W. S.; Wang, Z.; Li, Y.; Elimelech, M.; Jin, J.; Lin, S., Polyamide nanofiltration membrane with highly uniform sub-nanometre pores for sub-1 Å precision separation. *Nat. Commun.* **2020,** *11*, (1), 2015.
28. Kim, S. H.; Kwak, S. Y.; Suzuki, T., Positron annihilation spectroscopic evidence to demonstrate the flux-enhancement mechanism in morphology-controlled thin-film-composite (TFC) membrane. *Environ. Sci. Technol.* **2005,** *39*, (6), 1764-1770.
29. Louie, J. S.; Pinnau, I.; Reinhard, M., Gas and liquid permeation properties of modified interfacial composite reverse osmosis membranes. *J. Membr. Sci.* **2008,** *325*, (2), 793-800.
30. Lee, J.; Doherty, C. M.; Hill, A. J.; Kentish, S. E., Water vapor sorption and free volume in the aromatic polyamide layer of reverse osmosis membranes. *J. Membr. Sci.* **2013,** *425-426*, 217-226.
31. Pype, M. L.; Lawrence, M. G.; Keller, J.; Gernjak, W., Reverse osmosis integrity monitoring in water reuse: The challenge to verify virus removal - A review. *Water Res.* **2016,** *98*, 384-395.

32. Slipko, K.; Reif, D.; Wogerbauer, M.; Hufnagl, P.; Krampe, J.; Kreuzinger, N., Removal of extracellular free DNA and antibiotic resistance genes from water and wastewater by membranes ranging from microfiltration to reverse osmosis. *Water Res.* **2019,** *164*, 114916.
33. Adham, S.; Gagliardo, P.; Smith, D.; Ross, D.; Gramith, K.; Trussell, R., Monitoring the integrity of reverse osmosis membranes. *Desalination* **1998,** *119*, (1-3), 143-150.
34. Song, X.; Gan, B.; Qi, S.; Guo, H.; Tang, C. Y.; Zhou, Y.; Gao, C., Intrinsic nanoscale structure of thin film composite polyamide membranes: connectivity, defects, and structure-property correlation. *Environ. Sci. Technol.* **2020,** *54*, (6), 3559-3569.
35. Elimelech, M.; Zhu, X.; Childress, A. E.; Hong, S., Role of membrane surface morphology in colloidal fouling of cellulose acetate and composite aromatic polyamide reverse osmosis membranes. *J. Membr. Sci.* **1997,** *127*, (1), 101-109.
36. Pacheco, F. A.; Pinnau, I.; Reinhard, M.; Leckie, J. O., Characterization of isolated polyamide thin films of RO and NF membranes using novel TEM techniques. *J. Membr. Sci.* **2010,** *358*, (1), 51-59.
37. Peng, L. E.; Yao, Z.; Yang, Z.; Guo, H.; Tang, C. Y., Dissecting the role of substrate on the morphology and separation properties of thin film composite polyamide membranes: Seeing is believing. *Environ. Sci. Technol.* **2020,** *54*, (11), 6978-6986.
38. Song, X.; Gan, B.; Yang, Z.; Tang, C. Y.; Gao, C., Confined nanobubbles shape the surface roughness structures of thin film composite polyamide desalination membranes. *J. Membr. Sci.* **2019,** *582*, 342-349.
39. Peng, L. E.; Yang, Z.; Long, L.; Zhou, S.; Guo, H.; Tang, C. Y., A critical review on porous substrates of TFC polyamide membranes: Mechanisms, membrane performances, and future perspectives. *J. Membr. Sci.* **2022,** *641*, 119871.
40. Peng, L. E.; Gan, Q.; Yang, Z.; Wang, L.; Sun, P. F.; Guo, H.; Park, H. D.; Tang, C. Y., Deciphering the role of amine concentration on polyamide formation toward enhanced RO performance. *ACS EST Eng.* **2022,** *2*, (5), 903-912.
41. Zhu, J.; Hou, J.; Zhang, R.; Yuan, S.; Li, J.; Tian, M.; Wang, P.; Zhang, Y.; Volodin, A.; Van der Bruggen, B., Rapid water transport through controllable, ultrathin polyamide nanofilms for high-performance nanofiltration. *J. Mater. Chem. A* **2018,** *6*, (32), 15701-15709.
42. Sauerbrey, G., Verwendung von Schwingquarzen zur Wägung dünner Schichten und zur Mikrowägung. *Zeitschrift für physik* **1959,** *155*, (2), 206-222.
43. Zhang, X.; Cahill, D. G.; Coronell, O.; Mariñas, B. J., Absorption of water in the active layer of reverse osmosis membranes. *J. Membr. Sci.* **2009,** *331*, (1-2), 143-151.
44. Tang, C.; Kwon, Y.; Leckie, J., Probing the nano- and micro-scales of reverse osmosis membranes—A comprehensive characterization of physiochemical properties of uncoated and coated membranes by XPS, TEM, ATR-FTIR, and streaming potential measurements. *J. Membr. Sci.* **2007,** *287*, (1), 146-156.
45. Akin, O.; Temelli, F., Probing the hydrophobicity of commercial reverse osmosis membranes produced by interfacial polymerization using contact angle, XPS, FTIR, FE-SEM and AFM. *Desalination* **2011,** *278*, (1-3), 387-396.
46. Chen, D.; Werber, J. R.; Zhao, X.; Elimelech, M., A facile method to quantify the carboxyl group areal density in the active layer of polyamide thin-film composite membranes. *J. Membr. Sci.* **2017,** *534*, 100-108.

47. Coronell, O.; González, M. I.; Mariñas, B. J.; Cahill, D. G., Ionization behavior, stoichiometry of association, and accessibility of functional groups in the active layers of reverse osmosis and nanofiltration membranes. *Environ. Sci. Technol.* **2010,** *44*, (17), 6808-6814.
48. Chen, H.; Hung, W. S.; Lo, C. H.; Huang, S. H.; Cheng, M. L.; Liu, G.; Lee, K. R.; Lai, J. Y.; Sun, Y. M.; Hu, C. C.; Suzuki, R.; Ohdaira, T.; Oshima, N.; Jean, Y. C., Free-volume depth profile of polymeric membranes studied by positron annihilation spectroscopy: Layer structure from interfacial polymerization. *Macromolecules* **2007,** *40*, (21), 7542-7557.
49. Schultz, P. J.; Lynn, K. G., Interaction of positron beams with surfaces, thin films, and interfaces. *Reviews of Modern Physics* **1988,** *60*, (3), 701-779.
50. Gan, B.; Qi, S.; Song, X.; Yang, Z.; Tang, C. Y.; Cao, X.; Zhou, Y.; Gao, C., Ultrathin polyamide nanofilm with an asymmetrical structure: A novel strategy to boost the permeance of reverse osmosis membranes. *J. Membr. Sci.* **2020,** *612*.
51. Wen, Y.; Dai, R.; Li, X.; Zhang, X.; Cao, X.; Wu, Z.; Lin, S.; Tang, C. Y.; Wang, Z., Metal-organic framework enables ultraselective polyamide membrane for desalination and water reuse. *Sci. Adv.* **2022,** *8*, (10), eabm4149.
52. Freger, V.; Srebnik, S., Mathematical model of charge and density distributions in interfacial polymerization of thin films. *J. Appl. Polym. Sci.* **2003,** *88*, (5), 1162-1169.
53. Ji, J.; Dickson, J. M.; Childs, R. F.; McCarry, B. E., Mathematical model for the formation of thin-film composite membranes by interfacial polymerization: Porous and dense films. *Macromolecules* **2000,** *33*, (2), 624-633.
54. Chai, G. Y.; Krantz, W. B., Formation and characterization of polyamide membranes via interfacial polymerization. *J. Membr. Sci.* **1994,** *93*, (2), 175-192.
55. Matthews, T. D.; Yan, H.; Cahill, D. G.; Coronell, O.; Mariñas, B. J., Growth dynamics of interfacially polymerized polyamide layers by diffuse reflectance spectroscopy and Rutherford backscattering spectrometry. *J. Membr. Sci.* **2013,** *429*, 71-80.
56. Peng, L. E.; Jiang, Y.; Wen, L.; Guo, H.; Yang, Z.; Tang, C. Y., Does interfacial vaporization of organic solvent affect the structure and separation properties of polyamide RO membranes? *J. Membr. Sci.* **2021,** *625*, 119173.
57. Lin, L.; Lopez, R.; Ramon, G. Z.; Coronell, O., Investigating the void structure of the polyamide active layers of thin-film composite membranes. *J. Membr. Sci.* **2016,** *497*, 365-376.
58. Yan, H.; Miao, X.; Xu, J.; Pan, G.; Zhang, Y.; Shi, Y.; Guo, M.; Liu, Y., The porous structure of the fully-aromatic polyamide film in reverse osmosis membranes. *J. Membr. Sci.* **2015,** *475*, 504-510.
59. Yan, W.; Wang, Z.; Zhao, S.; Wang, J.; Zhang, P.; Cao, X., Combining co-solvent-optimized interfacial polymerization and protective coating-controlled chlorination for highly permeable reverse osmosis membranes with high rejection. *J. Membr. Sci.* **2019,** *572*, 61-72.
60. Kong, C.; Kanezashi, M.; Yamomoto, T.; Shintani, T.; Tsuru, T., Controlled synthesis of high performance polyamide membrane with thin dense layer for water desalination. *J. Membr. Sci.* **2010,** *362*, (1-2), 76-80.
61. Kurihara, M.; Sasaki, T.; Nakatsuji, K.; Kimura, M.; Henmi, M., Low pressure SWRO membrane for desalination in the Mega-ton Water System. *Desalination* **2015,** *368*, 135-139.

62. Grzebyk, K.; Armstrong, M. D.; Coronell, O., Accessing greater thickness and new morphology features in polyamide active layers of thin-film composite membranes by reducing restrictions in amine monomer supply. *J. Membr. Sci.* **2022,** *644*, 120112.
63. Avena, M. J.; Koopal, L. K.; van Riemsdijk, W. H., Proton binding to humic acids: Electrostatic and intrinsic interactions. *J. Colloid Interface Sci.* **1999,** *217*, (1), 37-48.
64. Tang, C. Y.; Kwon, Y. N.; Leckie, J. O., Fouling of reverse osmosis and nanofiltration membranes by humic acid—Effects of solution composition and hydrodynamic conditions. *J. Membr. Sci.* **2007,** *290*, (1), 86-94.
65. Zhang, F.; Wu, Y. P.; Li, W. X.; Xing, W. H.; Wang, Y., Depositing lignin on membrane surfaces for simultaneously upgraded reverse osmosis performances: An upscalable route. *AICHE J.* **2017,** *63*, (6), 2221-2231.
66. Kunihiro, H.; Takahiro, K., Method for improving rejection rate of reverse osmosis membrane. U.S. Patent US10046280B2. Aug. 14, 2018.
67. Jin, Y.; Wang, W.; Su, Z., Spectroscopic study on water diffusion in aromatic polyamide thin film. *J. Membr. Sci.* **2011,** *379*, (1), 121-130.
68. Ali, Z.; Wang, Y.; Ogieglo, W.; Pacheco, F.; Vovusha, H.; Han, Y.; Pinnau, I., Gas separation and water desalination performance of defect-free interfacially polymerized para-linked polyamide thin-film composite membranes. *J. Membr. Sci.* **2021,** *618*, 118572.
69. Freger, V., Kinetics of Film Formation by Interfacial Polycondensation. *Langmuir* **2005,** *21*, (5), 1884-1894.